

1 Dear Dr. Battin,

2 I wish you an happy new year and all the best for 2018.

3 You will find the new version of the manuscript « Molecular fingerprinting of particulate organic matter as a new
4 tool for its source apportionment: changes along a headwater drainage in coarse, medium and fine particles as a
5 function of rainfalls » modified according to the comments of the three anonymous reviewers.

6 In the following you will find a description of the modifications that were made. They are highlighted in green in
7 the text. I think that they have improved the quality and the readability of my paper.

8 Have a good day

9 Sincerely

10 Laurent Jeanneau

11 *On behalf of the coauthors*

12

13 Throughout the text : the acronyms for fatty acids (FA) and phenolic compounds (PHE) were removed. From the
14 beginning of the discussion section, the signification of the acronyms of the end members was reminded.
15 (Reviewers 1, 2 and 3)

16 In Table S1, the variables used for the statistical treatment were identified with the symbol *. (Reviewer 1)

17 The caption of the figures and tables have been modified to be self-explaining. (Reviewer 1)

18 The definition of what is POM in this study was added at paragraph 2.2. (Reviewer 2)

19 Two assumptions regarding the fact that some samples plotted outside the end-members triangle on figure 4 were
20 added at the end of the first paragraph of the section 3.5. (Reviewer 3)

21 About the comparison between molecular and isotopic data, a precision about this exercice was added at the end
22 of section 2.4. « using an end-member mixing approach » (Reviewer 3)

23 The following sentence :Such a method induces modification of the velocity profile around the sampler, which
24 could result in grain size fractionation. was added in section 2.2 to precise that the sampler is not isokinetic
25 (Reviewer 3; specific comment 1)

26 The word “mean” was replaced by “intermediate” in the section 3.1 for the description of Event 1 E1. (Reviewer
27 3; specific comment 2)

- 28 A precision about $n\text{-C}_{16:0}$ and $n\text{-C}_{18:0}$ that can derive from plant-derived inputs was added at the end of the section
29 3.3 (Reviewer 3; specific comment 5)
- 30 Mandatory was replaced by necessary at the end of the first paragraph of section 4.4. (Reviewer 3; specific
31 comment 6)
- 32 The data are now available in the supplementary files. (Reviewer 3; specific comment 7)

33 **Molecular fingerprinting of particulate organic matter as a new tool**
34 **for its source apportionment: changes along a headwater drainage in**
35 **coarse, medium and fine particles as a function of rainfalls**

36 Laurent Jeanneau^{1*}; Richard Rowland²; Shreeram Inamdar²

37 ¹ Univ rennes, CNRS, Geosciences Rennes - UMR 6118, F-35000 Rennes, France

38 ² Water Science & Policy Program, University of Delaware, Newark, USA

39 *Correspondence to:* Laurent Jeanneau (laurent.jeanneau@univ-rennes1.fr)

40 **Abstract.** Tracking the sources of particulate organic matter (POM) exported from catchments is important to understand the
41 transfer of energy from soils to oceans. The suitability of investigating the molecular composition of POM by thermally
42 assisted hydrolysis and methylation using tetramethylammonium hydroxide directly coupled to gas chromatography and
43 mass spectrometry is presented. The results of this molecular fingerprint approach were compared with previously published
44 elemental (%C, %N) and isotopic data ($\delta^{13}\text{C}$, $\delta^{15}\text{N}$) acquired in a nested headwater catchment in Piedmont region, Eastern
45 United States of America (12 and 79 ha). The concordance between these results highlights this molecular tool as a valuable
46 method for source fingerprinting of POM. It emphasizes litter as the main source of exported POM at the upstream location
47 (80 ± 14 %) with an increasing proportion of stream bed (SBed) sediments remobilization downstream (42 ± 29 %),
48 specifically during events characterized by high rainfall amounts. At the upstream location, the source of POM seems to be
49 controlled by the maximum and median hourly rainfall intensity. An added-value of this method is to directly investigate
50 chemical biomarkers and to mine their distributions in term of biogeochemical functioning of an ecosystem. In this
51 catchment, the distribution of plant-derived biomarkers characterizing lignin, cutin, and suberin inputs were similar in SBed
52 and litter, while the proportion of microbial markers was 4 times higher in SBed than in litter. These results indicate that
53 SBed OM was largely from plant litter that has been processed by the aquatic microbial community.

54 1 Introduction

55 Particulate organic matter (POM) plays key-roles in aquatic ecosystems, controlling the transfer and the bioavailability of
56 energy, nutrients and micropollutants. The flux of POM from soils to oceans has been estimated at 0.2 GtC per year (Ludwig
57 et al., 1996) with 80 % coming from biospheric inputs and the complement from petrogenic inputs (Galy et al., 2015).
58 Assuming that the energy provided by natural organic matter is equivalent of the energy provided by the combustion of
59 wood, this flux of POM corresponds to an energy of 2.8 EJ, that is to say less than 2 days of the global energy consumption
60 of 2015 (yearbook.enerdata.net). This export mainly occurs during storm events, those hot moments being responsible for up
61 to 80% of annual particulate organic carbon (POC) export depending on the investigated catchment (Dhillon and Inamdar,
62 2013; Jeong et al., 2012; Jung et al., 2012; Oeurng et al., 2011).

63 Among these hot moments, extreme events, defined as storm flow exceeded less than 10 % of the time (IPCC, 2001), seem
64 to play a dominant role. In two contrasted catchments, a mountainous one in South-Korea and a lowland one in the Eastern
65 United States of America (USA), the specific POC flux (flux per unit area of the catchment) has been shown to be non
66 linearly related to total rainfall with a threshold value beyond which the slope increased sharply (Dhillon and Inamdar, 2013;
67 Jung et al., 2014). The threshold value (approx. 70 mm in the American catchment and approx. 120 mm in the South-Korean
68 catchment) and the magnitude of this increase differed between both catchments and are probably watershed-dependant. Is
69 the non linearity of the relationship between rainfall amount and POC export observed previously linked to a modification of
70 the source of POM? POM in a river system is a combination of allochthonous and autochthonous OM. The former is derived
71 mainly from the soils and banks erosion, while the latter can be composed of fresh aquatic living organisms and bed
72 sediments. The balance between these different sources is controlled (i) by the catchment' size and morphology and (ii) by
73 the rainfall event characteristics (Tank et al., 2010).

74 Tracking the sources of POM can be done indirectly by investigating the sources of suspended matter. This can be done
75 through the analysis of fallout radionuclides such as Beryllium-7, Lead-210 and Cesium-137 (Ritchie et al., 1974; Wallbrink
76 and Murray, 1996; Walling, 1998) or by geochemical fingerprinting of rare elements (Collins and Walling, 2002). It can also
77 be done directly by investigating the composition of POM using bulk-scale descriptors such as OC and Nitrogen
78 concentrations, C/N ratio and stable isotopes $\delta^{13}\text{C}$ and $\delta^{15}\text{N}$ (Fox and Papanicolaou, 2008). Molecular biomarkers analyses
79 have also been used. They are based on specific molecular classes such as lipid or lignin biomarkers (Goñi et al., 2013; Jung
80 et al., 2015). Thermochemiolysis using tetramethylammonium hydroxide coupled to gas chromatography and mass
81 spectrometry has already been applied to the investigation of the fate of river DOM (Jeanneau et al., 2015) and POM
82 (Mannino and Harvey, 2000). This analytical technique is widely used to investigate the biogeochemistry of soil organic
83 matter (Derenne and Quénéa, 2015) and, coupled to a principal component analysis (PCA), it has been shown to be valuable
84 for forensic soils applications (Lee et al., 2012). An advantage of such an analysis is to generate a distribution of more than
85 hundred identified target compounds with small amount of particulate matter (from 5 to 10 mg) (Jeanneau et al., 2014),

86 giving a dataset rich enough to differentiate between sources (Walling, 2013). Here this analytical approach is combined with
87 a principal component analysis (PCA) to determine the main sources of POM as a function of the sediment size, the
88 catchment size and the rainfall characteristics.

89 The first objective of this paper is to test the suitability of molecular biomarkers derived from THM-GC-MS as a tool to
90 determine the sources of river POM. The second objective is to investigate how the sources of POM changed as a function of
91 the catchment size, particle size of the sediment, and the hydrological characteristics of the rainfall events. This study is
92 based on a subset of samples used to investigate the sources of POM exported during storm events using ^{13}C and ^{15}N as
93 tracers (Rowland et al., 2017). We hypothesized that molecular biomarkers provide important insights into sources of POM
94 and can be used as complimentary tracers for POM alongside or in addition to stable isotopes.

95 **2 Material and methods**

98 **1 Site description**

99 This study was conducted in a 79 ha watershed (second order stream) located in the Piedmont physiographic region of
100 Maryland, USA (Figure 1). The watershed drains into the Big Elk Creek which discharges into the Chesapeake Bay. For a
101 detailed description of the study site, refer to Rowland et al. (2017). Briefly, the watershed is predominantly forested with
102 pasture along the outer periphery. Dominant canopy species include *Fagus grandifolia* (American beech), *Liriodendron*
103 *tulipifera* (yellow poplar), and *Acer rubrum* (red maple). Bedrock formations consist of metamorphic gneiss and schist and
104 soils are coarse loamy, mixed, mesic lithic inceptisols on slopes and oxyaquic inceptisols in saturated valley bottoms.
105 Elevations in the watershed range from 77 to 108 m with slope gradients ranging from 0.16 to 24.5° (mean 6.3°). Mean
106 annual precipitation from 1981 to 2010 in this region was 1173.5 mm, with late spring and late summer as the wettest and
107 driest periods, respectively, and mean annual temperature is 13°C (Delaware State Climatologist Office Data Page, 2016).

111 **2.2 Watershed monitoring and sampling strategy**

112 Detailed information on monitoring and sampling is provided in Rowland et al. (2017). Climatological data was obtained
113 from a local station maintained by the Delaware Environmental Observing System approximately 450 m from the 79 ha
114 catchment outlet. This consists of temperature and GEONOR gage hourly rainfall measurements. Stream discharge estimates
115 were obtained at 20-minute intervals using a Parshall flume at 12 ha stream location (nested within the 79 ha watershed,
116 Figure 1) and a discharge rating curve calculated from paired pressure transducer and acoustic Doppler velocity meter
117 measurements at a rectangular concrete culvert at the 79 ha location.

118 Suspended sediments were collected using in-situ samplers made of 10 cm diameter capped PVC pipes placed vertically in
119 the middle of the stream. The upstream face of the pipes was perforated with 1.5 cm diameter holes beginning ~10 cm above

120 the stream bed. During periods of elevated discharge, stream stage rose above the perforations, trapping suspended sediment
121 within the sampler. The trapped sediment thus represented a time-integrated composite sediment sample (CSS). Such a
122 method induces modification of the velocity profile around the sampler, which could result in grain size fractionation. All
123 CSS were retrieved within 24 hours of the end of an event and frozen prior to processing and analysis. In this study POM
124 was defined by this sampler as the organic matter in the objects (natural debris, soil particles, colloids) that were trapped .
125 The slots on the samplers were approximately 1.5 cm which represents the higher threshold. The samples were dried before
126 further analysis and then included the smallest fractions defined as colloidal OM and dissolved OM.

127 Seven potential sediment sources were identified within the catchment and have been sampled at three locations to integrate
128 their spatial heterogeneity (Rowland et al., 2017). These included the stream bed (SBed), exposed stream bank A (BaA) and
129 B (BaB) horizons, valley-bottom wetland surficial soils (W), forest floor litter (Li) and humus (FH) and the upland A
130 horizons (Up). Sampling was conducted during the summer of 2015. 500-750 g of each end-member were sampled using an
131 ethanol-cleaned trowel or auger from both of the main tributary branches of the watershed. Stream beds were sampled from
132 areas without major backwatering or pooling, as POM may undergo diagenesis here, and were composited along a three by
133 three-point grid within the channel. Bank sediments were collected from exposed incised banks with three points composited
134 from the A and B horizons. Forest floor litter and humus, valley-bottom wetland soils and upland A horizons samples were
135 composited from five points along 20 m transects in low gradient locations in order to integrate their spatial heterogeneity.
136 End-member soil and sediment samples and CSS were dried in acid-cleaned Pyrex dishes in an oven at 45°C until visibly
137 dry. Oven-dry CSS samples were partitioned into coarse (CPOM) > 1000 µm, medium (MPOM) 1000-250 µm and fine
138 (FPOM) < 250 µm size classes via dry sieving. Dry masses were recorded for particle size class from which the fractional
139 mass percent was calculated for each class in each CSS sample. End-member samples were pre-sieved at 2 mm to remove
140 large organic debris such as roots. Aliquots were lyophilized overnight and preserved in a desiccator cabinet until elemental,
141 isotopic and molecular analyses. CSS and end-member samples were pulverized and homogenized using a ceramic mortar
142 and pestle that was cleaned with ethanol between samples.

143 2.3 Analytical methodology

144 For elemental and isotopic analyses, please refer to Rowland et al., (2017). The thermochemiolysis using
145 tetramethylammonium hydroxide (TMAH) coupled to gas chromatography and mass spectrometry (THM-GC-MS) was
146 performed according to Jeanneau et al. (2014). Briefly we introduced approximately 5 mg of freeze-dried solid residue into
147 an 80 µL aluminum reactor with an excess of solid TMAH (ca. 10 mg) and 10 µl of a solution of dihydrocinnamic acid d9
148 (CDN Isotopes, ref. D5666) diluted at 25 µg/ml in methanol as an internal standard. The THM reaction was performed on-
149 line using a vertical micro-furnace pyrolyser PZ-2020D (Frontier Laboratories, Japan) operating at 400°C. The products of
150 this reaction were injected into a gas chromatograph (GC) GC-2010 (Shimadzu, Japan) equipped with a SLB 5MS capillary
151 column in the split mode (60 m × 0.25 mm ID, 0.25 µm film thickness). The temperature of the transfer line was 321°C and
152 the temperature of the injection port was 310°C. The oven was programmed to maintain an initial temperature of 50°C for 2

153 minutes, then rise to 150°C at 15°C min⁻¹, and then rise to 310°C at 3 °C min⁻¹ where it stayed for 14 minutes. Helium was
154 used as the carrier gas, with a flow rate of 1.0 ml/min. Compounds were detected using a QP2010+ mass spectrometer (MS)
155 (Shimadzu, Japan) operating in the full scan mode. The temperature of the transfer line was set at 280°C, the ionization
156 source at 200°C, and molecules were ionized by electron impact using an energy of 70 eV. The list of analyzed compounds
157 and m/z ratios used for their integration are given in the supplementary materials (Table S1). Compounds were identified on
158 the basis of their full-scan mass spectra by comparison with the NIST library and with published data (Nierop et al., 2005;
159 Nierop and Verstraten, 2004). They were quantified assuming similar ionization and detection efficiencies between all
160 compounds. This assumption means that the concentrations must be handled as rough estimations.

161 Target compounds were classified into four categories: low molecular weight organic acids, phenolic compounds including
162 lignin and tannin markers, carbohydrates and fatty acids. The peak area of the selected m/z (mass/charge) for each compound
163 was integrated and corrected by a mass spectra factor calculated as the reciprocal of the proportion of the fragment used for
164 the integration and the entire fragmentogram provided by the NIST library (Table S1). The proportion of each compound
165 class was calculated by dividing the sum of the areas of the compounds in this class by the sum of the peak areas of all
166 analyzed compounds expressed as a percentage. The analytical uncertainty for this analytical method, expressed as a relative
167 standard deviation ranged from 10 to 20% depending on the samples and the target compounds. The use of THM-GC-MS to
168 investigate the sources of POM meant that it was necessary to assume that matrix effects are equivalent for all analyzed
169 compounds in all samples.

170 **2.4 Statistical analyses and calculation of the proportions of the main sources of POM in CSS**

171 Statistical analyses were performed using XLSTAT (version 19.01, Addinsoft). First a principal component analysis (PCA)
172 was performed using the end-members as individuals and CSS as additional individuals. The relative proportions of the 112
173 target compounds and the sum of their concentrations in ng/mg of freeze-dried matrix were used as variables. The relative
174 distribution of target compounds allows the direct comparison of the different samples without concentration effect, while
175 using the sum of their concentrations takes into consideration the fact that the concentration of target compounds differed
176 from a sample to another.

177 The first PCA allows identifying the correlated variables on the basis of a modulus of the Pearson coefficient > 0.9. When
178 two variables were correlated, the least abundant was removed. Then a second PCA was performed. The variables with a
179 correlation lower than 0.4 with the two first factors (F1: 29.8%; F2: 17.2% of variance) were removed, resulting in a new set
180 of 71 variables. A third PCA was calculated and a hierarchical ascendant classification (HAC) was calculated using the
181 coordinates of the individuals (end-members and CSS) on the 9 first factors that explained 90.5% of the variance of the
182 dataset. This HAC identified Upland soils and Stream bank sediments as minor contributors. Consequently a fourth PCA was
183 calculated removing Upland soils and Stream bank sediments from the potential end-members. Similarly to the three
184 previous PCA, CSS were considered as additional individuals. The coordinates of CSS on the two first factors (on 10) of this
185 PCA (F1: 40.1%; F2: 24.0% of variance) were used to calculate the proportion of the three main sources of POM in CSS

186 identified as 1. stream bed sediments, 2. litter and 3. forest floor humus + wetland soil, resolving a system of equations with
187 three unknowns. To solve this system, the coordinates of end-members must be specified. The heterogeneity of the
188 distribution of target compounds resulted in an area for each end-member. To calculate the proportions and uncertainties, the
189 coordinates of end-members were randomly selected ten times in the areas defined by the 95% IC. When the calculation
190 gave a negative contribution for an end-member, it was set at 0 and the two others contributions were recalculated to sum at
191 100. Finally the contributions of those three sources were approximated for the bulk POM by using the proportion and the
192 OC content of each fraction. From the third PCA to the end of the procedure, this treatment was also performed adding TOC,
193 $\delta^{13}\text{C}$ and $\delta^{15}\text{N}$ from Rowland et al. (2017) as variables.

194 In order to test the efficiency of the source apportionment calculated with the molecular data, the proportions of end
195 members and their isotopic values (Rowland et al., 2017) were used **in an end-member mixing approach** to model the $\delta^{13}\text{C}$ of
196 CSS. Modeled values were compared to measured values reported by Rowland et al. (2017) by calculating the relative
197 standard deviation (RSD) and against a linear regression model.

198 **3 Results**

200 **3.1 Rainfall and hydrology**

201 The molecular composition of POM in coarse, medium and fine size classes was investigated for four events. The rainfall
202 and discharge characteristics recorded for those events are indicated in Table 1. The total rainfall ranged from 40.1 (E4) to
203 148.9 (E1) mm, the maximum hourly rainfall (Imax) ranged from 19.9 (E1) to 31.3 (E3) mm h⁻¹ and the median hourly
204 rainfall (Imed) ranged from 0.4 (E3) to 2.2 (E2) mm h⁻¹. The maximum discharge for those events ranged from 15.6 (E4) to
205 150.1 (E1) l s⁻¹. Then the four events can be distinguished as follows. E1 was characterized by high rainfall, a low maximum
206 intensity (Imax), an **intermediate** median intensity (Imed) and an **intermediate** antecedent precipitation index (API7). E2 was
207 characterized by mean total rainfall, a mean Imax, a high Imed and a mean API7. E3 was characterized by high rainfall and
208 Imax, low Imed and high API7. Finally E4 was characterized by low rainfall and Imax, a high Imed and a dry antecedent
209 conditions (API7 = 0 mm). E2 and E4 were comparable in terms of precipitation regime but can be differentiated by the
210 API7, E4 occurring after 7 days without precipitation.

215 **3.2 Size distribution**

216 CSS were separated into coarse (>1 mm), medium (>250 μm) and fine (<250 μm) fractions, with the exception of CSS at the
217 downstream (79 ha) location for the fourth event (Table 1). In the 12 ha sub-catchment, the coarse, medium and fine
218 fractions represented 22 ± 20 , 22 ± 4 and 55 ± 21 % of particulate matter, respectively, while in the 79 ha catchment, they
219 represented 61 ± 19 , 22 ± 10 and 18 ± 10 % of particulate matter, respectively. In the 12 ha sub-catchment, the relative

220 standard deviation (RSD) of those proportions was 90, 17 and 37 % for the coarse, medium and fine fractions, respectively,
221 while in the 79 ha catchment it was 31, 45 and 55 %, respectively.

222 3.3 Molecular composition of end-members

223 The number of detected target compounds ranged from 49 (SBed#1) to 112 (FH). A Dixon test for extreme value identified
224 the lowest value (SBed#1) as an outlier (p -value = 0.011). Once this value removed, the number of detected target
225 compounds ranged from 75 (BaB) to 112 (FH). The low value recorded for one of the SBed could be due to a combination of
226 a low OC content with a low analytical efficiency. This sample was removed from the dataset.

227 The distribution of target compounds into chemical families gives a first overview of the molecular composition of OM in
228 the different end-members (Figure 2). In W, Li and FH, the main compounds are phenolic compounds and high molecular
229 weight fatty acids ($> C_{20}$, HMW) that represent more than 30% of target compounds. In BaA and BaB, the proportion of
230 phenolic compounds was lower (22 ± 4 and 19 ± 1 %, respectively; mean \pm SD) than in W, Li and FH and the proportion of
231 low molecular weight ($< C_{20}$, LMW) fatty acids was higher (27 ± 17 and 35 ± 9 %, respectively). In Up, compared to W, Li
232 and FH, the proportion of HMW fatty acids increased (57 ± 19 %), while the proportion of phenolic compounds decreased
233 (13 ± 8 %). In SBed, the main identified target compounds were LMW fatty acids (72 ± 8 %), while phenolic compounds
234 and HMW fatty acids represented 15 ± 2 % and 9 ± 4 %, respectively.

235 HMW fatty acids was composed of linear n -alkanoic acids from n -C_{20:0} to n -C_{32:0} with an even-over-odd predominance
236 characteristic of plant-derived inputs (Eglinton and Hamilton, 1967), linear ω -hydroxyacids and α,ω -diacids from n -C₁₆ to n -
237 C₂₈, 10,16-dihydroxyC_{16:0} and 9,10,18-trihydroxyC_{18:0} characteristic of plant-derived aliphatic biopolymers cutin and suberin
238 (Armas-Herrera et al., 2016; Kolattukudy, 2001). These two latter hydroxyacids were the main compounds among HMW
239 fatty acids. The proportion of ω -hydroxyacids and α,ω -diacids among HMW fatty acids is higher in roots than in leaves and
240 can be used to differentiate between suberin from roots and cutin from shoots (Mueller et al., 2012). This proportion
241 decreased from soils (Up, FH and W) and bank sediments to litter and was minimal for SBed (17 ± 8 %), highlighting that
242 the proportion of cutin decreased from SBed, Li to bank sediments and soils.

243 Phenolic compounds included of methoxy-benzene, -acetophenone, -benzaldehyde and -benzoic acids. These compounds
244 derived from lignin and tannins and are characteristic of plant-derived OM. The main compounds were guaiacyl-like
245 structures: 3,4-dimethoxybenzaldehyde, 3,4-dimethoxybenzoic acid methyl ester, *erythro* and *threo*-1,2-dimethoxy-4-(1,2,3-
246 trimethoxypropyl)benzene and syringil-like structures: 3,4,5-trimethoxybenzaldehyde and 3,4,5-trimethoxybenzoic acid
247 methyl ester, which is typical of the THM-GC-MS of OM deriving from woody plants (Challinor, 1995). Benzoic acid was
248 not classified in this chemical family since it was negatively (slope of the linear regression model: -0.20; -0.18; -0.17) and
249 poorly correlated (Pearson coefficient, p -value: 0.14, 0.002; 0.14, 0.002; 0.21, <0.001) with 3,4-dimethoxybenzoic acid
250 methyl ester, 3,4,5-trimethoxybenzoic acid methyl ester and 3-(3,4-dimethoxyphenyl)prop-2-enoic acid methyl ester,

251 respectively, that are the main representatives of the three types of lignin units analyzed by THM-GC-MS (Challinor, 1995).
252 As a consequence, it was not considered to calculate the proportion of molecules coming from lignins and tannins.
253 LMW acids included *n*-alkanoic acids from *n*-C_{6:0} to *n*-C_{19:0}, *iso* and *anteiso* C_{13:0}, C_{15:0} and C_{17:0}, *iso* C_{14:0} and C_{16:0} and *n*-
254 alkenoic acids *n*-C_{16:1} and *n*-C_{18:1}. The LMW fatty acids with less than 13 C atoms can derive from microbial or plant-derived
255 inputs, while the LMW fatty acids with more than 13 C atoms are known as phospholipid fatty acids and are microbial
256 biomarkers (Frostegård et al., 1993) with the exception of *n*-C_{16:0} and *n*-C_{18:0} that can derive from plant-derived inputs. The
257 proportion of microbial markers among target compounds was calculated according to Jeanneau et al. (2014). It increased
258 from litter and soils (<15%) to bank sediments (18 ± 12 % and 25 ± 7 % in BaA and BaB, respectively) to SBed (48 ± 15 %).

259 3.4 Molecular composition of stream suspended sediments

260 The distribution of target compounds into the five chemical families previously described changed with the catchment size as
261 illustrated on Figure 3. At the 12 ha location, this distribution was fairly homogenous across the particle classes. When
262 averaged across size fractions and events, the THM-GC-MS of the POM of CSS sampled at the 12 ha location mainly
263 produced phenolic compounds (48 ± 6 %, mean ± SD) and HMW fatty acids (22 ± 10 %). The relative standard deviation
264 weighted by the proportion (RSDp) was 13, 14 and 22 % for C, M and F fractions, respectively, which highlights a low inter-
265 event variability of this distribution. At the 79 ha location, the distribution of target compounds was dominated by LMW
266 fatty acids (41 ± 20 %) and phenolic compounds (37 ± 9 %). It was almost stable between the three size fractions with a
267 higher proportion of LMW fatty acids in the M fraction. However, the RSDp was 50, 55 and 23 % for C, M and F fractions,
268 respectively, which means a higher inter-event variability than at the 12 ha location.

276 3.5 End-members contributions

277 A hierarchical ascendant classification (HAC) was performed using the coordinates of end-members and stream sediments
278 (CSS) on the nine first factors (90.5 % of variance) of the PCA, which were calculated with the relative proportions of target
279 compounds and the sum of their concentrations as variables. Three classes were isolated. The first one included the three Li,
280 one FH and one W as end-members, the size fractions of CSS from the 12 ha location and 3 size fractions of CSS from the
281 79 ha location. The second group included two W, two FH and the three BaA, BaB and U end-members. Finally the third
282 group included the SBed end-members and the size fractions of CSS from the 79 ha location. Based on this HAC, Up, BaA
283 and BaB were considered as minor contributors to the POM exported from the 12 ha and 79 ha locations.

284 An additional PCA was then calculated using SBed, Li, FH and W as individuals, CSS as additional individuals, and the
285 previously defined list of 71 variables. The two first factors of this PCA explained 64.1 % of the variance of this final
286 dataset. The projection of end-members and CSS on the plan obtained with these two factors is illustrated on Figure 4. This
287 projection allows differentiating: (i) the three groups of end-members, Li, SBed and a combination of FH and W, denoted
288 FH-W and (ii) POM from the two sampling locations. Moreover the size classes were also separated. From this 2D
289 projection, an area was defined for each end-member corresponding to the 95% confidence interval. The results of the source

290 apportionment calculated using this 2D projection are listed in Table 2. Some CSS plotted outside the triangle formed by
291 end-members most probably because (1) the litter end-member did not capture the full compositional diversity of the
292 catchment and (2) end-member composition was investigated on bulk samples.

293 At the 12ha location, as an average of the four sampled events, from FPOM to CPOM, the proportion of OM coming from
294 SBed decreased from 17 ± 16 % (mean \pm SD) to 1 ± 1 %, the proportion of OM coming from FH-W decreased from 16 ± 16
295 % to 8 ± 12 % and the proportion of OM coming from Li increased from 67 ± 7 % to 90 ± 11 %. The large uncertainties
296 quantified by the mean RSD (78 ± 53 %, mean \pm SD, $n = 9$) reflected the inter-storm variability of this source
297 apportionment. Bulk POM was mainly inherited from Li with contributions ranging from 65 to 92 %.

298 At the 79ha location, as an average of the four sampled events, CPOM was mainly inherited from Li (63 ± 28 %) and SBed
299 (36 ± 30 %). MPOM was mainly due to SBed inputs (49 ± 39 %) and received a substantial contribution of FH-W (17 ± 31
300 %). Similarly to CPOM, FPOM was mainly inherited from Li (55 ± 15 %) and SBed (38 ± 24 %). Similarly to the source
301 apportionment at the 12ha location, the large uncertainties (RSD = 97 ± 57 %, $n = 9$) were due to inter-storm variability.
302 Bulk POM was mainly inherited from Li with contributions ranging from 42 to 89 % and SBed with contributions ranging
303 from 8 to 57 %.

304 4 Discussions

305 4.1 What are the main sources of POM for the watershed?

306 The HAC identified four main end-members for the stream water POM: litter (Li), the surface horizon of forest soils (FH)
307 and wetland soils (W) and stream bed sediments (SBed). Li was the main source of POM identified along the catchment
308 representing 80 ± 14 % and 49 ± 24 % of the POM exported from the 12 ha and 79 ha catchments, respectively. These high
309 proportions of Li-derived POM is in accordance with the results of Jung et al. (2015) where isotopic and *n*-alkanes
310 fingerprints of POM exported from a mountainous forested headwater catchment highlighted similarities with litter and
311 surface soils. Moreover the decrease in the proportion of Li-derived OM along the catchment fits well with the observation
312 of Koiter et al. (2013) where the contribution of topsoil sources of suspended sediments decreased from 75 to 30 % when
313 moving downstream.

314 Stream bank A and B horizons and the surface horizons of upland soils did not group with any CSS, which would mean that
315 they were minor contributors for the investigated samples. This seems to be in contradiction with the documented impact of
316 bank erosion on the mobilization of particulate organic matter (Adams et al., 2015; Nosrati et al., 2011; Tamooh et al., 2012).
317 This apparent contradiction could be due to the catchment's size. Contrary to the previously cited investigations (Adams et
318 al., 2015; Nosrati et al., 2011; Tamooh et al., 2012), this present study focused on a headwater catchment (0.79 km²). In these
319 small catchments, POM mainly comes from the erosion of surrounding soils as observed for monsoon floods in Laos
320 (Gourdin et al., 2015; Huon et al., 2017) or from a combination of bedrock and surface erosion in an Alpine catchment with

321 relative proportions controlled by the precipitations (Smith et al., 2013). However, in this catchment, the mobilization of
322 stream banks has been shown to be effective in winter due to freeze-thaw process (Inamdar et al., 2017). This present study
323 analyzed four events sampled in spring and summer. The lower contribution of stream bank erosion could then be due to
324 seasonal variability.

325 The relative proportion of phenolic compounds compared to HMW fatty acids plotted against the proportion of α,ω -diacids
326 and ω -hydroxyacids with more than 20 C atoms among HMW fatty acids resulted in a visual differentiation of Li and SBed
327 from wetland (W), forest humus (FH), River bank horizons A (BaA) and B (BaB) and from Upland soil (Up) (Figure 5). This
328 observation highlights Li as the main origin of SBed plant-derived OM, which fits well with the high proportion of Li-
329 derived POM in CSS from both catchments. Moreover from Li to SBed, (i) the ratio of coumaric and ferulic acids to
330 vanillaldehyde, acetovanillone and vanillic acid, commonly noted C/V, decreased from 0.79 ± 0.26 to 0.20 ± 0.07 , denoted
331 that lignins were more biodegraded in SBed than in Li and (ii) the proportion of microbial markers among the target
332 compounds increased from 12 ± 5 to 48 ± 15 %. Both of these observations highlight the recycling of terrestrial plant-
333 derived OM in river sediments from a headwater catchment, and are in accordance with the higher mineralization rate of soil
334 organic carbon in river sediments (Wang et al., 2014).

340 4.2 Are molecular data in accordance with isotopic and elemental data?

341 A four-step analysis was performed to determine if the molecular data produced by THM-GC-MS were in accordance with
342 the isotopic results (Rowland et al., 2017) previously acquired on those samples.

343 The first one consists in a point-by-point comparison of the source apportionments resulting from the two approaches. Four
344 main observations were reported by Rowland et al. (2017) using the isotopic approach. First, “the litter layer was a dominant
345 contributor to CPOM, especially for the upstream locations”. This is in agreement with our data: the proportion of Li-derived
346 CPOM was 90 ± 11 % and 63 ± 28 % for the 12ha and the 79ha catchments, respectively. Secondly, “the proportional
347 contributions of SBed and banks to MPOM and FPOM increased downstream”. This is also in agreement with molecular
348 data, however stream banks were not considered as a main contributor through the present statistical treatment. The
349 proportion of SBed-derived POM increased from 8 ± 8 % to 49 ± 39 % and from 17 ± 16 % to 38 ± 24 % between the 12 ha
350 and the 79 ha catchments in MPOM and FPOM, respectively. Thirdly, “no appreciable shift was observed in CPOM source”.
351 This is partly in agreement with the molecular data. The main contributor to CPOM was Li in the two locations but the
352 proportion of SBed-derived CPOM increased downstream. Finally, the highest contribution of forest floor humus was
353 observed in MPOM and FPOM for E4. This is in agreement with the source apportionment in this study since the proportion
354 of FH-W-derived POM was the highest for this event in CPOM, MPOM and FPOM from the 12 ha catchment and in MPOM
355 and FPOM from the 79 ha catchment.

356 In a second step, the quality of the source apportionment calculated from the end member mixing approach was investigated
357 by modeling the $\delta^{13}\text{C}$ of the samples using the isotopic fingerprint of end members. These modeled values were compared to

358 the measured values used in the isotopic fingerprinting approach (Rowland et al., 2017). The relative standard deviation was
359 1.1 ± 0.2 % (mean \pm 95% CI; $n = 20$) and the linear regression resulted in a slope of 1.01 ($R^2 = 0.58$; p -value < 0.0001 ;
360 Figure S1) highlighting a fairly good agreement between the model and the data, that is to say between the source
361 apportionment using molecular data and measured $\delta^{13}\text{C}$.

362 In a third step, TOC, $\delta^{13}\text{C}$, $\delta^{15}\text{N}$ and C/N were added as variables in the PCA treatment. In a first PCA, W, FH, Li, SBed,
363 BaA, BaB and Up were considered as potential end members. A HCA using the nine first PCA factors (90.4 % of the
364 variance) highlighted BaA, BaB and Up as minor contributors, similarly to this step performed on molecular data alone.
365 Then a second PCA was calculated with FH, W, Li and SBed as potential end members and the CSS as additional
366 individuals. The two first factors represented 64.4 % of the variance and resulted in a clear differentiation between Li, SBed
367 and FH-W. The same approach was then applied using the molecular data alone, resulting in the calculation of the
368 proportions of those three end members in the CSS for ten different combinations of the position of end members in the 2D
369 plan created by the two first factors of the PCA. For each CSS sample a set of ten values was created for Li-, SBed- and FH-
370 W-derived POM (Table S2). Student T-test was used to compare these distributions between the modality “molecular data”
371 and the modality “molecular + isotopic, elemental data”. A p -value was calculated for each sample. They ranged from 0.08 to
372 0.49 (0.25 ± 0.03 ; mean \pm 95% CI), highlighting that there were no significant differences between the two approaches
373 (Table S3).

374 The final step aimed at investigating to what extent the molecular data are representative of bulk POM. The linear regression
375 between the sum of the concentrations of target compounds (expressed in $\mu\text{g/g}$ of dry solid) and the total organic content
376 (expressed in % of dry solid) resulted in a correlation coefficient of 0.94 (p -value < 0.0001 ; Figure S2). This correlation
377 between bulk scale and molecular analyses has already been highlighted for sedimentary and dissolved OM (Jeanneau and
378 Faure, 2010; Jeanneau et al., 2014) and emphasizes the suitability of molecular investigations to determine the sources of
379 OM.

380 Once validated by this four-step comparison, what are the insights provided by the molecular approach on the source
381 apportionment of CPOM, MPOM and FPOM along this Piedmont headwater catchment?

382 **4.3 Modification of the source apportionment as a function of rainfall parameters**

383 These present results may be valuable to investigate the relationships between the sources of exported POM and rainfall
384 characteristics. However they have been acquired on only four events and this part of the discussion should be enriched by
385 future investigations.

386 Rainfall is the primary driver for C export since it controls soil erosion and stream discharge (Raymond and Oh, 2007).
387 Rainfall amount and API7 have been shown to control the export of POC from headwater catchments (Dhillon and Inamdar,
388 2013, 2014; Jung et al., 2014). Moreover Imax and Imed have also been identified as important drivers for soil erosion since

389 they control the rainfall erosivity (Wischmeier, 1959). The four investigated events represented a range of rainfall amounts,
390 maximal hourly intensity (I_{max}), median hourly intensity (I_{med}) and antecedent precipitation index (API7).
391 Linear regression were performed between the proportions of Li-, SBed- and FH-W-derived POM in CPOM, MPOM and
392 FPOM from both catchments against rainfall amount, I_{max} , I_{med} and API7 (Table 1). With only four investigated events,
393 only relationships characterized by Pearson coefficient higher than 0.8 were considered. p -Values were not calculated for
394 those regressions since they would not have had any statistical value. With only four events the highlighted relationships
395 must be handled with care and may be seen as guidelines for future works.

396 In the 12 ha catchment, SBed-derived OM was positively related to I_{max} and API7 and negatively related to I_{med} . The
397 positive relationship with API7 was recorded in C and F fractions, while the positive relationship with I_{max} and the negative
398 relationship with I_{med} were recorded only in the F fraction. In the M fraction, SBed-derived OM was related to the total
399 rainfall. However since this fraction represented 22 ± 4 % (mean \pm SD) of the exported particles, this relationship was not
400 considered as representative. In the 12 ha catchment the export of SBed-derived OM would be favored by rainfall
401 characterized by high I_{max} occurring after a period of dryness (Figure 6a). Moreover the proportion of FH-W-derived OM
402 was positively related to I_{med} in F fraction. This fraction represented 55 ± 21 % (mean \pm SD) of the exported particles,
403 giving some representativity to this observation. A deeper analysis of the relationship between I_{med} and the proportion of
404 FH-W-derived OM in the different fractions from the 12 ha catchment highlights a concomitant control of API7 (Figure 6b).
405 For similar I_{med} (E2 versus E4), the proportion of FH-W-derived OM increased in the three fraction with dry antecedent
406 conditions. The activation of the soil reservoir seems to be controlled by both I_{med} and API7, which could be interpreted as
407 the necessity of a dry period to replenish a stock of soil OM available for soil erosion and that intensive and regular rainfalls
408 could result in higher soil erosion.

409 In the 79 ha catchment, the proportions of Li and FH-W were negatively related to the rainfall amount and the proportion of
410 SBed was positively related to this variable. These relationships were recorded in the C and M fractions, with the exception
411 of FH-W (only in the C fraction). A deeper analysis of the link between the POM source apportionment and the rainfall
412 amount highlights different threshold values for C, M and F fractions (Figure 6c). In M and F fractions, there was a sharp
413 modification of the source of POM between E4 (40.1 mm) and E2 (43.9 mm). The proportion of FH-W-derived POM
414 decreased from 64 ± 20 % to 0 ± 1 % and from 21 ± 22 % to 1 ± 2 %, in the M and F fractions, respectively. These decreases
415 were concomitant with increases in the proportion of SBed-derived POM from 0 ± 0 % to 43 ± 8 % and from 2 ± 2 % to $48 \pm$
416 9 %, in the M and F fractions, respectively. The source apportionment of FPOM remained unchanged by further increases of
417 the rainfall amount, while for MPOM the source apportionment was clearly modified during E1, which was characterized by
418 the highest rainfall amount (148.9 mm). The proportion of Li-derived POM decreased to 0 ± 1 % and the proportion of
419 SBed-derived POM increased from 58 ± 9 % to 95 ± 7 %. The source apportionment of CPOM drastically changed between
420 E2 and E3 (97.4 mm). The proportion of Li-derived POM decreased from 95 ± 8 % to 47 ± 9 % and the proportion of SBed-
421 derived POM increased from 2 ± 4 % to 53 ± 9 %. This source apportionment remained unchanged between E3 and E1.
422 Since the C fraction was the most important during events 1, 2 and 3, its source apportionment was an important driver of the

423 source of total POM. It was mainly modified between events 2 and 3 with a decrease in the proportion of Li-derived POM
424 and an increase in the proportion of SBed-derived POM. From these observations, the threshold value of 75 mm previously
425 found in this catchment with an increase in the slope of the POC exported in kg/ha as a function of the rainfall amount
426 (Dhillon and Inamdar, 2013) falls in the range from 43.9 mm (E2) to 97.4 mm (E3), where the main modifications of the
427 source of POM exported from the 79 ha catchment were observed. The increase in the proportion of SBed-derived POM
428 accompanied with the increase in the proportion of the C fraction could be the result of the exceeding of a threshold value of
429 the hydrodynamism for sediment remobilization.

430 **4.4 Benefits and limitations of this molecular fingerprinting approach**

431 The present molecular fingerprinting method has benefits and limitations. Among the benefits, when the analysis is
432 performed on-line, that is to say, when the products of the THM are directly sent to the GC, then the analysis needs low
433 sample mass, in the order of 5 to 10 mg. Then this method is based on the molecular composition of OM, which is perfectly
434 suitable to investigate the fate of POM. Moreover it takes advantage of the differences of chemical composition between
435 living organisms (microorganisms versus plants) and in their different parts (leaves versus roots). As a consequence the
436 recorded modifications can be discussed in term of biogeochemistry of POM.

437 However limitations must be considered. Seasonal variability of the molecular fingerprint could exist especially for quickly
438 reactive reservoir such as litter (Williams et al., 2016). In soils, the turnover of OM takes time (> 50 years; Frank et al.,
439 2012). Consequently their molecular fingerprints may be less sensitive to seasonal variations, with the exception of
440 agricultural soils subject to changes in vegetation cover. This limitation can be easily avoided by sampling the most reactive
441 end-members at different seasons. The second and third limitations come from the method itself. First this is a time-
442 consuming method because each compound must be determined with care in each sample. For an analysis, approximately
443 two hours are **necessary**. Finally, because it is not only a value given by an analytical tool, using it asks having an expertise
444 in organic geochemistry.

445 When benefits and limitations are well considered, this molecular fingerprinting approach may be particularly suitable to
446 investigate the sources of POM in combination with other fingerprinting approaches.

447 **5 Conclusion**

448 This study emphasizes the suitability of molecular analysis of POM using THM-GC-MS to investigate the sources of POM
449 in headwater catchments. This analytical technique needs less than 5 mg of freeze-dried matter, which makes it realistic in
450 regard of the amount of suspended sediment exported and simple with only freeze-drying as a preparing step. With
451 approximately hundred of target compounds, the provided chemical fingerprint allows for the differentiation of the main
452 sources of exported POM, specifically between litter, surface soils, and in-channel sediments. The fairly good relationships
453 obtained by comparison with the conclusions gained by the isotopic-elemental investigation provide additional evidence in

454 favor of this organic fingerprinting approach. The present data highlight plant litter as the main source of exported POM with
455 an increasing contribution of stream bed sediments downstream. This latter contribution seems to be controlled by the
456 rainfall amount with a threshold phenomenon already observed for quantitative data. The contribution of soil erosion could
457 be controlled by both the median intensity of rainfall and the amount of rain in the previous 7 days. The investigation of
458 additional events in different catchments will be necessary to determine if those results are generic.

459 **Data availability**

460 Data are available on request from the corresponding author.

461 **Acknowledgements**

462 This study was funded by NSF ESPCoR Grant # IIA 1330238 (NEWNet) and USDA NIFA Grant # 2015-67020-23585. We
463 would like to thank the Fair Hill Natural Resources Management Area for allowing us to conduct this study in the Fair Hill
464 Nature Preserve. Many thanks to students who assisted with sampling including Erin Johnson, Catherine Winters, Chelsea
465 Krieg, Shawn Del Percio, Margaret Orr and Daniel Warner. **The authors also thank the three anonymous reviewers who**
466 **participate in the improvement of the quality of this paper.**

467 **References**

- 468 Adams, J. L., Tipping, E., Bryant, C. L., Helliwell, R. C., Toberman, H. and Quinton, J.: Aged riverine particulate organic
469 carbon in four UK catchments, *Sci. Total Environ.*, 536, 648–654, doi:10.1016/j.scitotenv.2015.06.141, 2015.
- 470 Armas-Herrera, C. M., Dignac, M.-F., Rumpel, C., Arbelo, C. D. and Chabbi, A.: Management effects on composition and
471 dynamics of cutin and suberin in topsoil under agricultural use, *Eur. J. Soil Sci.*, 67(4), 360–373, doi:10.1111/ejss.12328,
472 2016.
- 473 Challinor, J. M.: Characterisation of wood by pyrolysis derivatisation—gas chromatography/mass spectrometry, *J. Anal.*
474 *Appl. Pyrolysis*, 35(1), 93–107, doi:10.1016/0165-2370(95)00903-R, 1995.
- 475 Collins, A. . and Walling, D. .: Selecting fingerprint properties for discriminating potential suspended sediment sources in
476 river basins, *J. Hydrol.*, 261(1), 218–244, doi:10.1016/S0022-1694(02)00011-2, 2002.
- 477 Derenne, S. and Quéneá, K.: Analytical pyrolysis as a tool to probe soil organic matter, *J. Anal. Appl. Pyrolysis*, 111, 108–
478 120, doi:10.1016/j.jaap.2014.12.001, 2015.
- 479 Dhillon, G. S. and Inamdar, S.: Extreme storms and changes in particulate and dissolved organic carbon in runoff: Entering
480 uncharted waters?, *Geophys. Res. Lett.*, 40(7), 1322–1327, doi:10.1002/grl.50306, 2013.

481 Dhillon, G. S. and Inamdar, S.: Storm event patterns of particulate organic carbon (POC) for large storms and differences
482 with dissolved organic carbon (DOC), *Biogeochemistry*, 118(1), 61–81, doi:10.1007/s10533-013-9905-6, 2014.

483 Fox, J. F. and Papanicolaou, A. N.: Application of the spatial distribution of nitrogen stable isotopes for sediment tracing at
484 the watershed scale, *J. Hydrol.*, 358(1), 46–55, doi:10.1016/j.jhydrol.2008.05.032, 2008.

485 Frank, D. A., Pontes, A. W. and McFarlane, K. J.: Controls on Soil Organic Carbon Stocks and Turnover Among North
486 American Ecosystems, *Ecosystems*, 15(4), 604–615, doi:10.1007/s10021-012-9534-2, 2012.

487 Frostegård, Å., Tunlid, A. and Bååth, E.: Phospholipid Fatty Acid Composition, Biomass, and Activity of Microbial
488 Communities from Two Soil Types Experimentally Exposed to Different Heavy Metals, *Appl. Environ. Microbiol.*, 59(11),
489 3605–3617, 1993.

490 Galy, V., Peucker-Ehrenbrink, B. and Eglinton, T.: Global carbon export from the terrestrial biosphere controlled by erosion,
491 *Nature*, 521(7551), 204–207, 2015.

492 Goñi, M. A., Hatten, J. A., Wheatcroft, R. A. and Borgeld, J. C.: Particulate organic matter export by two contrasting small
493 mountainous rivers from the Pacific Northwest, U.S.A., *J. Geophys. Res. Biogeosciences*, 118(1), 112–134,
494 doi:10.1002/jgrg.20024, 2013.

495 Gourdin, E., Huon, S., Evrard, O., Ribolzi, O., Bariac, T., Sengtaheuanghoung, O. and Ayrault, S.: Sources and export of
496 particle-borne organic matter during a monsoon flood in a catchment of northern Laos, *Biogeosciences*, 12(4), 1073–1089,
497 doi:10.5194/bg-12-1073-2015, 2015.

498 Huon, S., Evrard, O., Gourdin, E., Lefèvre, I., Bariac, T., Reyss, J.-L., Henry des Tureaux, T., Sengtaheuanghoung, O.,
499 Ayrault, S. and Ribolzi, O.: Suspended sediment source and propagation during monsoon events across nested sub-
500 catchments with contrasted land uses in Laos, *J. Hydrol. Reg. Stud.*, 9, 69–84, doi:10.1016/j.ejrh.2016.11.018, 2017.

501 Inamdar, S., Johnson, E., Rowland, R., Warner, D., Walter, R. and Merritts, D.: Freeze–thaw processes and intense rainfall:
502 the one-two punch for high sediment and nutrient loads from mid-Atlantic watersheds, *Biogeochemistry*, doi:
503 10.1007/s10533-017-0417-7, 2017.

504 IPCC, 2001. *Climate Change. The IPCC Third Assessment Report. Volumes I (Science), II (Impacts and Adaptation) and III*
505 *(Mitigation Strategies)*. Cambridge Univ Press, Cambridge.

506 Jeanneau, L., Jaffrezic, A., Pierson-Wickmann, A.-C., Gruau, G., Lambert, T. and Petitjean, P.: Constraints on the Sources
507 and Production Mechanisms of Dissolved Organic Matter in Soils from Molecular Biomarkers, *Vadose Zone J.*, 13(7),
508 doi:10.2136/vzj2014.02.0015, 2014.

509 Jeanneau, L., Denis, M., Pierson-Wickmann, A.-C., Gruau, G., Lambert, T. and Petitjean, P.: Sources of dissolved organic
510 matter during storm and inter-storm conditions in a lowland headwater catchment: constraints from high-frequency
511 molecular data, *Biogeosciences*, 12(14), 4333–4343, doi:10.5194/bg-12-4333-2015, 2015.

512 Jeong, J.-J., Bartsch, S., Fleckenstein, J. H., Matzner, E., Tenhunen, J. D., Lee, S. D., Park, S. K. and Park, J.-H.: Differential
513 storm responses of dissolved and particulate organic carbon in a mountainous headwater stream, investigated by high-

514 frequency, in situ optical measurements, *J. Geophys. Res. Biogeosciences*, 117(G3), n/a-n/a, doi:10.1029/2012JG001999,
515 2012.

516 Jung, B.-J., Lee, H.-J., Jeong, J.-J., Owen, J., Kim, B., Meusburger, K., Alewell, C., Gebauer, G., Shope, C. and Park, J.-H.:
517 Storm pulses and varying sources of hydrologic carbon export from a mountainous watershed, *J. Hydrol.*, 440, 90–101,
518 doi:10.1016/j.jhydrol.2012.03.030, 2012.

519 Jung, B.-J., Lee, J.-K., Kim, H. and Park, J.-H.: Export, biodegradation, and disinfection byproduct formation of dissolved
520 and particulate organic carbon in a forested headwater stream during extreme rainfall events, *Biogeosciences*, 11(21), 6119–
521 6129, doi:10.5194/bg-11-6119-2014, 2014.

522 Jung, B.-J., Jeanneau, L., Alewell, C., Kim, B. and Park, J.-H.: Downstream alteration of the composition and
523 biodegradability of particulate organic carbon in a mountainous, mixed land-use watershed, *Biogeochemistry*, 122(1), 79–99,
524 doi:10.1007/s10533-014-0032-9, 2015.

525 Koiter, A. J., Lobb, D. A., Owens, P. N., Peticrew, E. L., Tiessen, K. H. D. and Li, S.: Investigating the role of connectivity
526 and scale in assessing the sources of sediment in an agricultural watershed in the Canadian prairies using sediment source
527 fingerprinting, *J. Soils Sediments*, 13(10), 1676–1691, doi:10.1007/s11368-013-0762-7, 2013.

528 Kolattukudy, P.: Polyesters in Higher Plants, in *Biopolyesters*, vol. 71, edited by W. Babel and A. Steinbüchel, pp. 1–49,
529 Springer Berlin Heidelberg. [online] Available from: http://dx.doi.org/10.1007/3-540-40021-4_1, 2001.

530 Lee, C. S., Sung, T. M., Kim, H. S. and Jeon, C. H.: Classification of forensic soil evidences by application of THM-
531 PyGC/MS and multivariate analysis, *J. Anal. Appl. Pyrolysis*, 96, 33–42, doi:10.1016/j.jaap.2012.02.017, 2012.

532 Ludwig, W., Probst, J.-L. and Kempe, S.: Predicting the oceanic input of organic carbon by continental erosion, *Glob.*
533 *Biogeochem. Cycles*, 10(1), 23–41, doi:10.1029/95GB02925, 1996.

534 Mannino, A. and Harvey, H. R.: Terrigenous dissolved organic matter along an estuarine gradient and its flux to the coastal
535 ocean, *Org. Geochem.*, 31(12), 1611–1625, doi:10.1016/S0146-6380(00)00099-1, 2000.

536 Mueller, K. E., Polissar, P. J., Oleksyn, J. and Freeman, K. H.: Differentiating temperate tree species and their organs using
537 lipid biomarkers in leaves, roots and soil, *Org. Geochem.*, 52, 130–141, doi:10.1016/j.orggeochem.2012.08.014, 2012.

538 Nierop, K. G. J. and Verstraten, J. M.: Rapid molecular assessment of the bioturbation extent in sandy soil horizons under
539 pine using ester-bound lipids by on-line thermally assisted hydrolysis and methylation-gas chromatography/mass
540 spectrometry, *Rapid Commun. Mass Spectrom.*, 18(10), 1081–1088, doi:10.1002/rcm.1449, 2004.

541 Nierop, K. G. J., Preston, C. M. and Kaal, J.: Thermally Assisted Hydrolysis and Methylation of Purified Tannins from
542 Plants, *Anal. Chem.*, 77(17), 5604–5614, doi:10.1021/ac050564r, 2005.

543 Nosrati, K., Govers, G., Ahmadi, H., Sharifi, F., Amoozegar, M. A., Merckx, R. and VanMaerke, M.: An exploratory study on
544 the use of enzyme activities as sediment tracers: biochemical fingerprints?, *Int. J. Sediment Res.*, 26(2), 136–151,
545 doi:10.1016/S1001-6279(11)60082-6, 2011.

546 Oeurng, C., Sauvage, S., Coynel, A., Maneux, E., Etcheber, H. and Sánchez-Pérez, J.-M.: Fluvial transport of suspended
547 sediment and organic carbon during flood events in a large agricultural catchment in southwest France, *Hydrol. Process.*,
548 25(15), 2365–2378, doi:10.1002/hyp.7999, 2011.

549 Raymond, P. A. and Oh, N.-H.: An empirical study of climatic controls on riverine C export from three major U.S.
550 watersheds, *Glob. Biogeochem. Cycles*, 21(2), n/a-n/a, doi:10.1029/2006GB002783, 2007.

551 Ritchie, J. C., Spraberry, J. A. and McHenry, J. R.: Estimating Soil Erosion from the Redistribution of Fallout ¹³⁷Cs₁, *Soil*
552 *Sci. Soc. Am. J.*, 38(1), 137–139, doi:10.2136/sssaj1974.03615995003800010042x, 1974.

553 Rowland, R., Inamdar, S. and Parr, T.: Evolution of particulate organic matter (POM) along a headwater drainage: role of
554 sources, particle size class, and storm magnitude, *Biogeochemistry*, 133(2), 181–200, doi:10.1007/s10533-017-0325-x, 2017.

555 Smith, J. C., Galy, A., Hovius, N., Tye, A. M., Turowski, J. M. and Schleppei, P.: Runoff-driven export of particulate organic
556 carbon from soil in temperate forested uplands, *Earth Planet. Sci. Lett.*, 365, 198–208, doi:10.1016/j.epsl.2013.01.027, 2013.

557 Tamoo, F., Van den Meersche, K., Meysman, F., Marwick, T. R., Borges, A. V., Merckx, R., Dehairs, F., Schmidt, S.,
558 Njunja, J. and Bouillon, S.: Distribution and origin of suspended matter and organic carbon pools in the Tana River Basin,
559 Kenya, *Biogeosciences*, 9(8), 2905–2920, doi:10.5194/bg-9-2905-2012, 2012.

560 Tank, J. L., Rosi-Marshall, E. J., Griffiths, N. A., Entekin, S. A. and Stephen, M. L.: A review of allochthonous organic
561 matter dynamics and metabolism in streams, *J. North Am. Benthol. Soc.*, 29(1), 118–146, doi:10.1899/08-170.1, 2010.

562 Wallbrink, P. J. and Murray, A. S.: Distribution and Variability of ⁷Be in Soils Under Different Surface Cover Conditions and
563 its Potential for Describing Soil Redistribution Processes, *Water Resour. Res.*, 32(2), 467–476, doi:10.1029/95WR02973,
564 1996.

565 Walling, D. E.: Use of ¹³⁷Cs and other fallout radionuclides in soil erosion investigations: progress, problems and prospects,
566 Joint FAO/IAEA Division of Nuclear Techniques in Food and Agriculture, International Atomic Energy Agency (IAEA),
567 Vienna (Austria). [online] Available from:
568 http://www.iaea.org/inis/collection/NCLCollectionStore/_Public/29/049/29049354.pdf, 1998.

569 Walling, D. E.: The evolution of sediment source fingerprinting investigations in fluvial systems, *J. Soils Sediments*, 13(10),
570 1658–1675, doi:10.1007/s11368-013-0767-2, 2013.

571 Wang, X., Cammeraat, E. L. H., Romeijn, P. and Kalbitz, K.: Soil Organic Carbon Redistribution by Water Erosion – The
572 Role of CO₂ Emissions for the Carbon Budget, *PLOS ONE*, 9(5), e96299, doi:10.1371/journal.pone.0096299, 2014.

573 Williams, J. S., Dungait, J. A. J., Bol, R. and Abbott, G. D.: Contrasting temperature responses of dissolved organic carbon
574 and phenols leached from soils, *Plant Soil*, 399, 13–27, doi:10.1007/s11104-015-2678-z, 2016.

575 Wischmeier, W. H.: A Rainfall Erosion Index for a Universal Soil-Loss Equation¹, *Soil Sci. Soc. Am. J.*, 23(3), 246–249,
576 doi:10.2136/sssaj1959.03615995002300030027x, 1959.

577 **Figure captions**

578 Figure 1: Location of the study watershed in the Piedmont region of Maryland. Composite suspended sediments were
579 sampled at the 12 and 79 ha locations (grey circles). The sites of collection of end-members are indicated with triangles:
580 violet for **wetland soils** (Wet), blue for **bed sediments** (SBed), green for **forest soil humus** (FH) and **litter** (Li), orange for
581 **upland soils** (Up) and yellow for **bank sediments from horizons A and B** (BaA and BaB).

582 Figure 2: Relative proportions of low organic acids (LOA), phenolic compounds (PHE), low molecular weight and high
583 molecular weight fatty acids (LMW and HMW FA) and carbohydrates (CAR) among identified target compounds in the end
584 members. Uncertainties correspond to standard deviation of sampling triplicates (duplicates for bed sediments SBed).

585 Figure 3: Relative proportions of low organic acids (LOA), phenolic compounds (PHE), low molecular weight and high
586 molecular weight fatty acids (LMW and HMW FA) and carbohydrates (CAR) among identified target compounds in the
587 coarse, medium and fine fractions of CSS. Uncertainties correspond to the inter-event standard deviation.

588 Figure 4: Plan defined by the two first factors of the PCA calculated using the distribution of target compounds. Squares
589 represent end members Li (green), FH-W (red) and SBed (blue). The area characteristic of each end member is defined by the
590 95% confident interval. Circles represent CSS from the 12 ha (orange) and the 79 ha (purple) locations. The mean positions
591 for each size fraction are represented by large circles and uncertainties correspond to inter-event standard deviation.

592 Figure 5: 2D plot illustrating the variability of the distribution of plant-derived markers using the relative proportion of
593 **phenolic compounds** (PHE) against HMW **fatty acids** and the proportion of α,ω diacids and ω OH fatty acids among HMW
594 **fatty acids** (denoted HMW FA ratio).

595 Figure 6: Illustration of the most significant correlations between the source apportionments performed using the molecular
596 data and rainfall characteristics. At the 12 ha location, positive correlations (a) between the proportion of Sbed-derived POM
597 and I_{max} and (b) between the proportion of FH-W-derived POM and I_{med}. At the 79 ha location, positive correlation
598 between Sbed-derived POM and rainfall amount (c). Coarse, medium and fine fractions are depicted by the dark grey, light
599 grey and white circles, respectively and the composite POM by the black diamond.

Table 1. Rainfall characteristics, discharge and proportion of coarse, medium and fine fractions for the 4 investigated storm events.

	Event 1		Event 2		Event 3		Event 4	
	<i>May 1, 2014</i>		<i>Apr. 21, 2015</i>		<i>July 3, 2015</i>		<i>Sept. 30, 2015</i>	
Rainfall								
total (mm)	148.9		43.9		97.4		40.1	
max (mm h ⁻¹)	19.9		20		31.3		20.2	
median (mm h ⁻¹)	1.3		2.2		0.4		2.1	
API7 (mm)	9.7		10.4		68.2		0	
Discharge (12 ha catchment)								
max (l s ⁻¹)	150.1		68.3		87.4		15.5	
Particle size distribution								
	<i>12 ha</i>	<i>79 ha</i>	<i>12 ha</i>	<i>79 ha</i>	<i>12 ha</i>	<i>79 ha</i>	<i>12 ha</i>	<i>79 ha</i>
Coarse (%)	52	81	20	43	12	58	6	nd
Medium (%)	22	13	22	32	27	20	18	nd
Fine (%)	27	7	59	25	61	21	75	nd

600

601

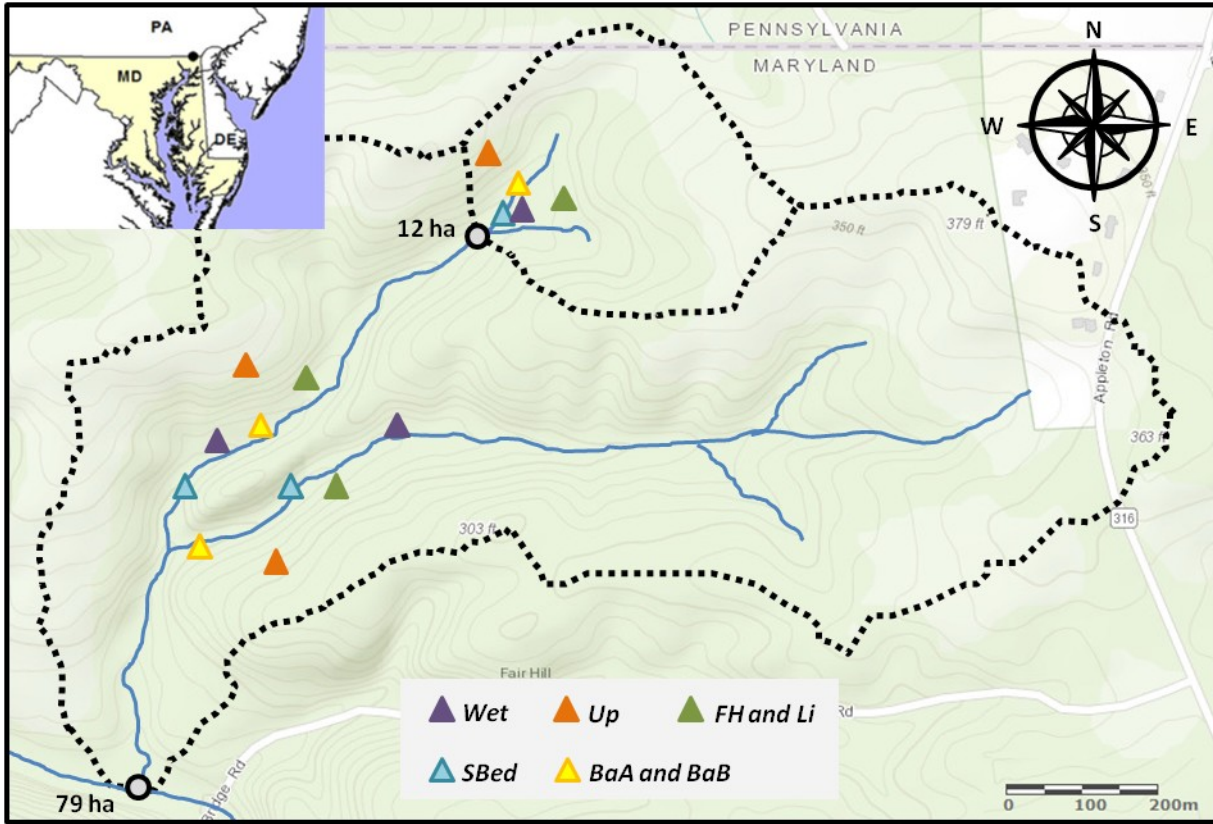
Table 2. Source apportionment calculated using the molecular data.

		<i>12 ha location</i>			<i>79 ha location</i>		
		Li (%)	Sbed (%)	FH-W (%)	Li (%)	Sbed (%)	FH-W (%)
Event 1 <i>May 1, 2014</i>	C	97 ± 7	1 ± 2	3 ± 7	45 ± 9	55 ± 9	0 ± 0
	M	78 ± 7	18 ± 5	4 ± 8	0 ± 1	95 ± 7	4 ± 7
	F	76 ± 12	13 ± 6	11 ± 16	48 ± 9	52 ± 9	0 ± 0
	POM	92 ± 9	4 ± 4	4 ± 11	42 ± 6	57 ± 8	0 ± 2
Event 2 <i>Apr. 21, 2015</i>	C	95 ± 8	2 ± 3	3 ± 8	95 ± 8	2 ± 4	3 ± 8
	M	94 ± 9	2 ± 3	4 ± 9	57 ± 9	43 ± 8	0 ± 1
	F	69 ± 16	15 ± 6	17 ± 20	51 ± 10	48 ± 9	1 ± 2
	POM	86 ± 11	6 ± 4	8 ± 12	89 ± 9	8 ± 7	3 ± 4
Event 3 <i>July 3, 2015</i>	C	96 ± 5	3 ± 4	1 ± 5	47 ± 9	53 ± 9	0 ± 0
	M	87 ± 6	10 ± 5	3 ± 7	42 ± 9	58 ± 9	0 ± 0
	F	61 ± 8	39 ± 7	0 ± 1	45 ± 11	51 ± 9	4 ± 6
	POM	81 ± 6	17 ± 6	2 ± 4	46 ± 10	53 ± 9	2 ± 2
Event 4 <i>Sept. 30, 2015</i>	C	73 ± 22	0 ± 0	27 ± 22	fraction not available		
	M	70 ± 22	0 ± 0	30 ± 22	36 ± 20	0 ± 0	64 ± 22
	F	62 ± 23	0 ± 0	38 ± 23	77 ± 20	2 ± 2	21 ± 22
	POM	65 ± 23	0 ± 0	35 ± 23	-	-	-

602

603

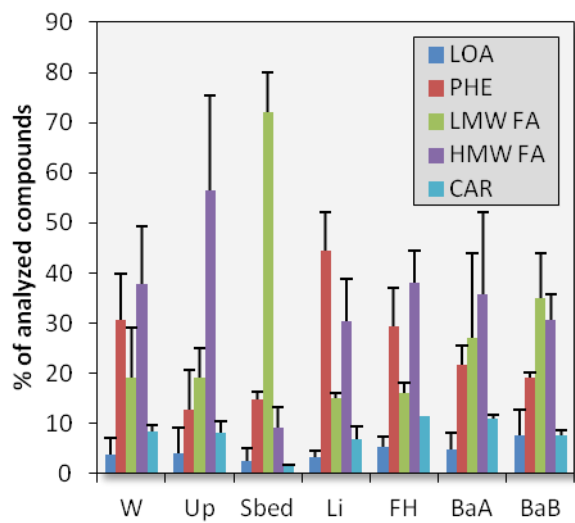
604 Figure 01



605

606

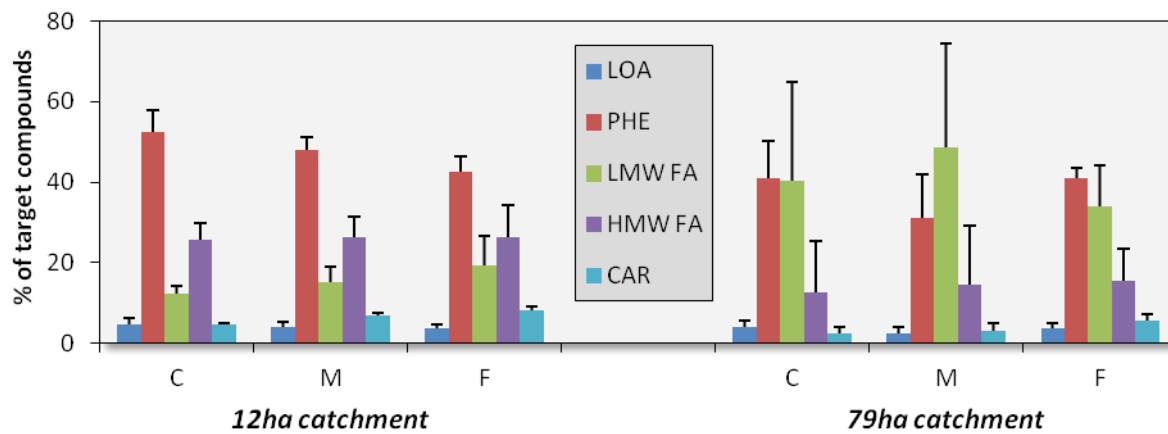
607 **Figure 02**



608

609

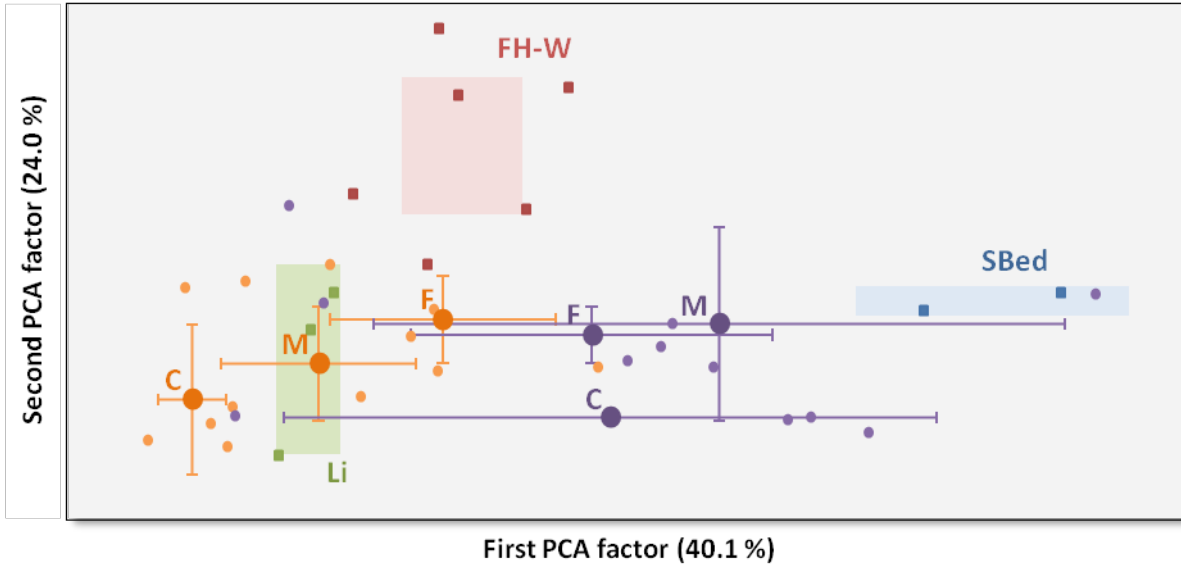
610 **Figure 03**



611

612

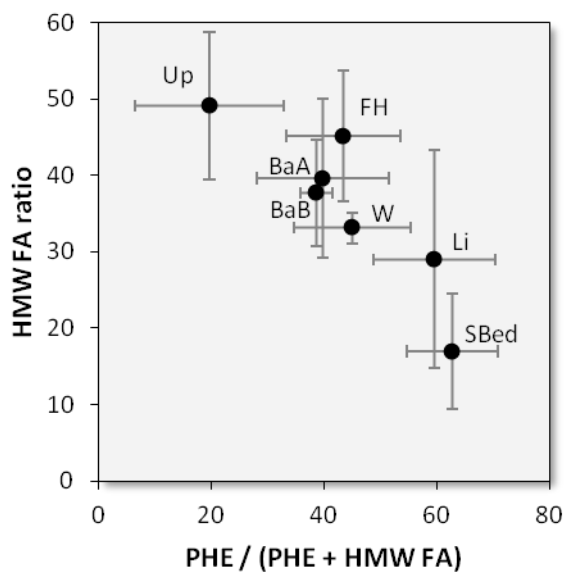
613 Figure 04



614

615

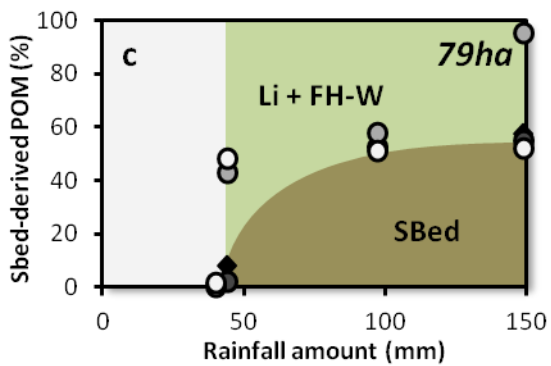
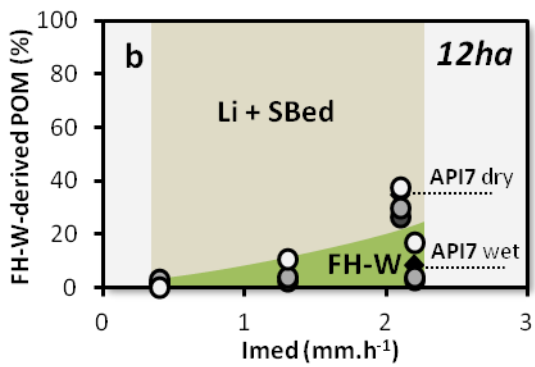
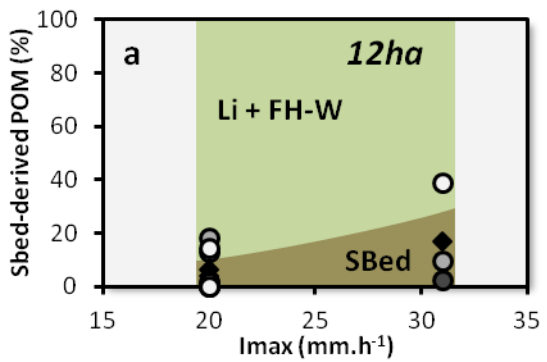
616 **Figure 05**



617

618

619 **Figure 06**



620

621

622